Increasing the efficiency of graphene-based Schottky barrier devices

Shuo-En Wu, Ya-Ping Hsieh*

Institute of Atomic and Molecular Sciences, Academia Sinica, Taipei 11617, Taiwan

*Corresponding author: E-mail: yphsieh@gate.sinica.edu.tw

DOI: 10.5185/amlett.2019.2183
www.vbripress.com/aml

Abstract

Graphene's high carrier mobility and ambipolar nature has the potential to improve electronic devices. The absence of a band-gap necessitates heterostructure devices. Schottky-barrier devices consisting of an interface between graphene and a semiconductor represent the simplest heterostructure. Despite its simplicity, graphene-based Schottky barrier devices are not well understood and exhibit low injection efficiencies. We here investigate the impact of graphene/metal interaction on the properties of the Schottky-barrier. Besides the commonly employed Au/graphene we use Pt/graphene contacts. We find that the injection efficiency for Pt is 5x higher than for Au and systematically study the origin of this behavior. We identify a large difference in the Richardson's constant due to changes in the density of surface states. The demonstrated ability to increase the injection current was applied to improve the efficiency of graphene-based Schottky solar cells by 13x. Copyright © 2019 VBRI Press.

Keywords: Graphene, Schottky barrier, Richardson, solar cell.

Introduction

Graphene is a two-dimensional carbon allotrope that is heralded as an enabling material for electronics [**1**] due to several attractive properties. Graphene exhibits a high carrier mobility in excess of 200,000 cm^2/V_s and shows ambipolar transport [**2, 3]**. A challenge for digital electronics, however, is the absence of a band-gap resulting in large leakage currents and low switching ratios. To overcome this issue, heterojunctions between graphene and semiconductors are the focus of significant research effort [**4, 5, 6, 7**]. Especially, novel atomically thin heterojunction devices could enable high performance electronic [**8**]. Finally, Schottky barrier devices have been used to produce solar cells with tunable absorption and efficiency [**9**].

Despite the attractiveness of graphene-based Schottky devices and the invested research effort, the efficiency of graphene-based Schottky injectors is significantly lower than bulk Schottky injectors [**6**]. This issue causes low current densities in Schottky devices and low conversion efficiency in Schottky solar cells [**10**]. Furthermore, the effect of interaction of graphene with metals used as contacts or dopants is expected to modify the Schottky barrier but limited insight exists [**9**].

We here investigate the effect of graphene/metal hybridization on the carrier transport across a Schottky barrier. Careful extraction of interface resistance and non-idealities reveals that neither factor can explain the differences between Pt/graphene and Au/graphene contacts. Instead, a large increase in the Richardson's constant for Pt/graphene is found and explained by changes to graphene's density of states. The improved carrier transport was applied to enhancing the solar cell efficiency of graphene Schottky solar cells by 10x.

Experimental

Graphene was grown by chemical vapor deposition following previous reports. Briefly, Cu-foil was electro polished and annealed at 1000 ℃ for 70 minutes and 10 sccm hydrogen. Then, methane was introduced at 10 sccm to initiate graphene growth. After 6 h the methane supply was shut off and the chamber was cooled down under hydrogen. Silicon substrates (resistivity: 1-50 Ω-cm) were cleaned and SiO_2 ring was deposited using shadow masked e-beam evaporation. (**Fig. 1a**). Graphene was transferred to Silicon substrates using PMMA transfer [**11**]. Metal films were deposited on top of the graphene by e-beam evaporation or wet-chemical methods ($AuCl_3$ in IPA solvent was dropped onto graphene). Contacts were produced by silver paste. Current-voltage characteristics were obtained using a B2912A source meter.

Results and discussion

Fig. 1b shows a representative current-voltage characteristic between graphene and n-type Silicon. The expected exponential increase of current with voltage is hidden by a large series resistance that results in an almost linear IV curve. Common Schottky diodes exhibit small series resistances which can be ignored. Similar assumptions had been made for graphene devices and

only the low-bias-regions were investigated [**6, 12**]. Instead, we include contributions by the series resistance $\boldsymbol{R_s}$ to a voltage lowering according to equation 1 [**13**].

$$\boldsymbol{I = I_s \exp\left(\frac{q(V-IR_S)}{nkT}\right)} \qquad \text{(eq. 1)}$$

Here $\boldsymbol{I_s}$ is the saturation current that contains contributions from injection barrier height $\boldsymbol{\phi_B}$ and Richardson's constant $\boldsymbol{A^*}$.

$$\boldsymbol{I_S = A_{eff} * A^* T^2 * \exp\left(-\frac{q\phi_B}{kT}\right)}$$

We follow the method by Cheung *et al.* [**13**] to extract the series resistance. **Fig. 1c** shows a plot of $\boldsymbol{dV/d(\ln(I))}$ vs. $\boldsymbol{I}$. The slope of this plot reveals the series resistance while the intercept corresponds to the ideality factor $\boldsymbol{nkT/q}$. While the method is straightforward and the good agreement of the plot to a linear dependence supports its applicability, not all-important parameters can be extracted. **Fig. 1d** shows the calculated IV curve from eq 1 using the extracted parameters and assuming a Richardson's constant of $\boldsymbol{A^*_{Si} = 112 \frac{A}{cm^2 K^2}}$. The inadequacy of the fit suggests that the Richardson's constant has to be a fitting parameter as well. We therefore use a second fitting process to improve the correctness of the parameters. For this purpose, the VI curve was fit to equation 2 using the parameters extracted by Cheung's method as starting point.

$$\boldsymbol{V = RI + n\phi_B + \frac{nkT}{q}\ln\left(\frac{I}{A_{eff}A^*T^2}\right)} \qquad \text{(eq. 2)}$$

We observe an improved fit (**Fig. 1d** and $\boldsymbol{R^2 > 0.99}$ was found for all devices. (Interestingly, ideality factor and series resistance of both methods agree within 2% error, highlighting the usefulness of Cheung's method).

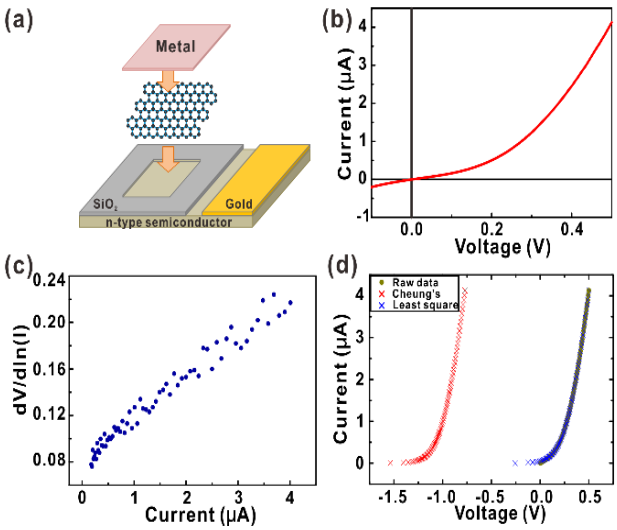

Fig. 1. (a) Schematic sample structure, (b) representative IV characteristics (c) dV/dln(I) vs I, (d) fits to Cheung's method and optimized least square fit.

The extended fitting procedure allows us to investigate the effects of different graphene/metal hybrids on the Schottky-barrier conduction. We use Au as a first metal because its interaction with graphene and the resulting Schottky barriers are well investigated. Pt was used as a second material and both material's Schottky parameters were extracted. We first focus on the extracted values of series resistance.

Fitting reveals that Au/graphene/n-Si structures exhibit series resistances of 7kΩ while Pt/graphene/n-Si only shows Rs values of 2kΩ. This difference is not related to the graphene resistance which is consistently below 500Ω. Instead, it suggests a significant difference in interfacial quality. To elucidate the behavior, we carry out temperature dependent measurements of Au and Pt covered Schottky diodes. We observe that the series resistance decreases with increasing temperature as expected for the contact resistance between graphene and Si according to eq. 3

$$\boldsymbol{\rho_c = \frac{k}{A^* Tq}\exp\left(\frac{q\phi_{In}}{kT}\right)} \qquad \text{(eq. 3)}$$

Surprisingly, however, from an Arrhenius plot we extract similar barriers for both Pt and Au covered graphene (0.23eV. and 0.22eV for Pt and Au, respectively (**Fig. 2a**). The difference in contact resistance is therefore another indicator that the deviation of the Richardson's constant is the reason for the observed behavior.

To investigate the differences between Au and Pt-covered graphene Schottky diodes we analyze the ideality factor n. While this parameter is around 1 for Pt covered graphene, it is approximately 3 for Au-covered graphene. Furthermore, the ideality factor shows a clear temperature-dependence (**Fig. 2b**). This behavior suggests that inhomogeneity in the barrier height across the sample occurs [**14**].

To confirm this hypothesis, we extract the barrier height dependence on temperature. Following Werner *et al.* [**15**] we plot the barrier height as a function of inverse temperature (**Fig. 2c**). We observe linear

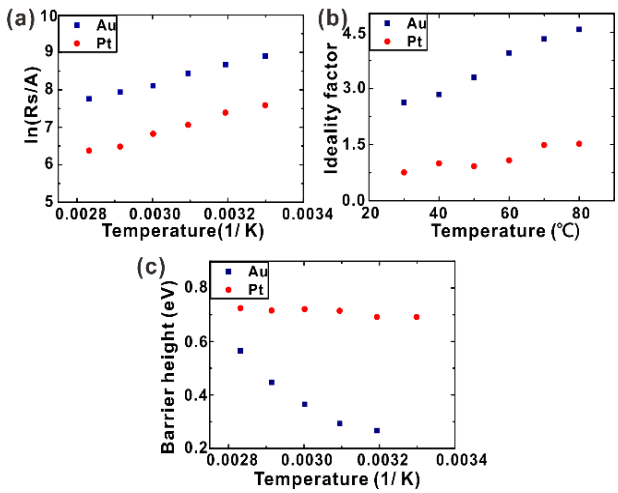

Fig. 2. Temperature dependence of (a) resistance, (b) ideality and (c) barrier.

behaviors for both Au and Pt in the plot. From these trends we can extract the standard deviation of the barrier height $\boldsymbol{\sigma_S}$ according to eq 4.

$$\boldsymbol{\phi_{measured} = \phi_b - \frac{q\sigma_S^2}{kT}} \qquad \text{(eq. 4)}$$

We extract values for $\boldsymbol{\sigma_S}$ of 1V and 3V for Pt and Au, respectively which are significantly larger than previous reports of bare grapheme [**14**].

We now attempt to explain the origin of the inhomogeneity of the barrier height by investigating the Richardson's constant A*. **Fig. 3a** shows A* vs. 1/T for both Au and Pt. Surprisingly completely different behaviors are extracted. For Au, the Richardson's constant decreases exponentially whereas for Pt A* increases linearly. Sinha *et al.*[**6**] employed the Landauer formalism to relate A* to the Density of states of graphene $\boldsymbol{D_0}$ and the temperature:

$$\boldsymbol{A^* = \frac{qD_0}{\tau} k_B^2 \left(\frac{\phi_B}{k_B T} + 1\right)} \qquad \text{(eq. 5)}$$

We find that Pt fits the predicted temperature dependence very well indicating that the injection current is indeed controlled by the density of states of graphene. The exponential decay in A* for Au, however, is not captured by equation 5. Future studies will have to establish if the observed temperature dependence originates from modulations of the coupling constant $\boldsymbol{\tau}$.

We now focus on understanding the relation of A* with the properties of Pt. **Fig. 3b** shows an increase of A* with increasing Pt thickness. This can be understood when comparing the graphene work function with varying amounts of Pt. Hall effect measurements reveal an increasing carrier concentration with increasing Pt thickness that can be related to graphene's work function by equation 6.

$$\boldsymbol{E_F = \hbar v_F \sqrt{\pi n}} \qquad \text{(eq. 6)}$$

Fig. 3c shows a decreasing work function that will cause a larger equilibrium barrier and thus increase the driving force of carrier injection according to equation 5.

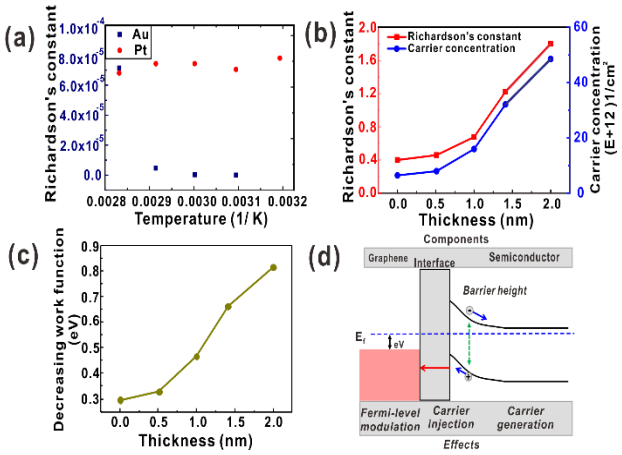

Fig. 3. (a)A* vs. 1/T for Au and Pt, (b) the relation of the A* and carrier concentration with the Pt thickness, (c) decreasing work function vs. Pt thickness, (d) schematic proposed mechanism.

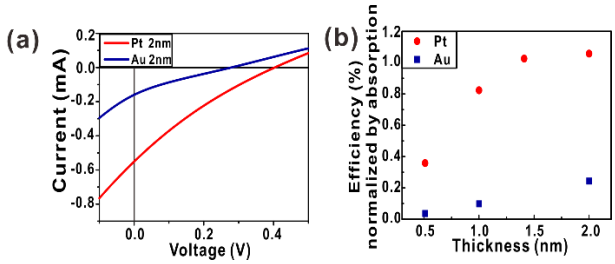

Fig. 4. (a) Solar cell IV curve with 2 nm Pt or Au, (b) efficiency/absorption vs. Pt or Au thickness.

Finally, we apply the gained insight to improving the efficiency of graphene-based Schottky barrier solar cells. We observe that the Pt covered graphene produces significantly larger short circuit currents compared to Au covered graphene (**Fig. 4a**). This behavior is in agreement with the previously found enhancement of the injection current in Pt.

In order to enhance the injection current, thicker Pt films are desirable. However, the thicker Pt films will also increase absorption and thus decrease the solar cell efficiency. We therefore show the efficiency normalized by the transmittance in **Fig. 4b**. We find that Pt covered graphene indeed exhibits an increasing trend with increasing Pt thickness. Furthermore, the normalized solar cell efficiency is 5 times larger for Pt than for Au-covered graphene. These results highlight the potential of improving the injection across the semiconductor/ graphene interface and open up new routes towards high efficiency graphene-based solar cells.

Conclusion

In conclusion, we have used Pt to enhance the efficiency of current injection across the graphene/n-Si interface. A lower inhomogeneity in barrier height was found compared to Au-covered graphene that indicates a higher quality of the interface. A larger equilibrium barrier between Si and Pt/graphene was found responsible for the enhanced Richardson's constant. This improvement results in a 13x larger efficiency of graphene-based Schottky solar cells.

Acknowledgements

The acknowledgements come at the end of an article after the conclusions and before the notes and references.

Supporting information

Supporting informations are available from VBRI Press.

References

1 Novoselov, K. S.; Fal, V.; Colombo, L.; Gellert, P.; Schwab, M.; Kim, K., *Nature*, **2012,** *490*, 192. **DOI:** 10.1038/nature11458
2 Chen, J. H.; Jang, C.; Xiao, S.; Ishigami, M.; Fuhrer, M. S., *Nature nanotechnology*, **2008,** *3*, 206. **DOI:** 10.1038/nnano.2008.58
3 Latil, S.; Henrard, L., *Physical Review Letters*, **2006**, *97*, 036803. **DOI:** 10.1103/PhysRevLett.97.036803
4 Yang, H.; Heo, J.; Park, S.; Song, H. J.; Seo, D. H.; Byun, K. E.; Kim, P.; Yoo, I.; Chung, H. J.; Kim, K., *Science*, **2012,** *336*, 1140. **DOI:** 10.1126/science.1220527

5 Kim, S.; Seo, T. H.; Kim, M. J.; Song, K. M.; Suh, E. K.; Kim, H., *Nano Research*, **2015,** 8, 1327.
DOI: 10.1007/s12274-014-0624-7

6 Sinha, D.; Lee, J. U., *Nano Letters*, **2014**, *14*, 4660.
DOI: 10.1021/nl501735k

7 Di, Bartolomeo, A., *arXiv preprint arXiv:1505.07686*, **2015**.
DOI: 10.1016/j.physrep.2015.10.003

8 Yu, W. J.; Li, Z.; Zhou, H.; Chen, Y.; Wang, Y.; Huang, Y.; Duan, X., *Nature materials*, **2013**, *12*, 246.
DOI: 10.1038/nmat3518

9 Shi, Y.; Kim, K. K.; Reina, A.; Hofmann, M.; Li, L. J.; Kong, J., *ACS nano*, **2010,** *4*, 2689.

10 Li, X.; Zhu, H.; Wang, K.; Cao, A.; Wei, J.; Li, C.; Jia, Y.; Li, Z.; Li, X.; Wu, D., *Advanced Materials*, **2010**, *22*, 2743.
DOI: 10.1002/adma.200904383

11 Li, X.; Zhu, Y.; Cai, W.; Borysiak, M.; Han, B.; Chen, D.; Piner, R. D.; Colombo, L.; Ruoff, R. S., *Nano Letters*, **2009**, *9*, 4359.
DOI: 10.1021/nl902623y

12 Chen, C. C.; Aykol, M.; Chang, C. C.; Levi, A.; Cronin, S. B., *Nano Letters*, **2011**, *11*, 1863.
DOI: 10.1021/nl104364c

13 Cheung, S.; Cheung, N., *Applied Physics Letters*, **1986**, *49*, 85.
DOI: 10.1063/1.97359

14 Tomer, D.; Rajput, S.; Hudy, L.; Li, C.; Li, L., *Nanotechnology*, **2015**, *26*, 215702.
DOI: 10.1088/0957-4484/26/21/215702

15 Werner, J. H.; Güttler, H. H., *Journal of Applied Physics*, **1991**, *69*, 1522.
DOI: 10.1063/1.347243s

